Slumped Glass Optics with interfacing ribs for high angular resolution X-ray astronomy: a progress report

M. Civitani[a,1], S. Basso[a], C.Brizzolari[a,b], M. Ghigo[a], G. Pareschi[a], B. Salmaso[a], D. Spiga[a], G.Vecchi[a], E.Breuning[c], V. Burwitz[c], G. D. Hartner[c], B. Menz[c]

[a]INAF Astronomical Observatory of Brera, Via E. Bianchi 46, I-23807 Merate (LC), Italy
[b]Università degli Studi dell'Insubria, Via Valleggio 11, 22100 Como, Italy
[c]Max-Planck-Institüt für extraterrestrische Physik (Germany)

ABSTRACT

The Slumped Glass Optics technology, developed at INAF/OAB since a few years, is becoming a competitive solution for the realization of the future X-ray telescopes with a very large collecting area, as e.g. the proposed Athena, with more than 2 m² effective area at 1 keV and with a high angular resolution (5" HEW). The developed technique is based on modular elements, named X-ray Optical Units (XOUs), made of several layers of thin foils of glass, previously formed by direct hot slumping in cylindrical configuration, and then stacked in a Wolter-I configuration, through interfacing ribs. The achievable global angular resolution of the optics relies on the surface shape accuracy of the slumped foils, on the smoothness of the mirror surfaces and on the correct integration and co-alignment of the mirror segments achieved with a dedicated Integration Machine (IMA). In this paper we provide an update of the project development, reporting on the last results achieved. In particular, we will present the results obtained with full illumination X-ray tests for the last developed prototypes.

Keywords: X-ray grazing-incidence telescopes, replication techniques, X-ray segmented mirrors, hot slumping of glass foils, integration and alignment of space optics,

1 Introduction

The Slumped Glass Optics (SGO) is being developed at INAF/OAB as an option to realize future X-ray telescopes, like Athena, combining large effective area and high angular resolution [1]. Due to the size of the mirror assembly to be realized, X-ray Optical Units (XOU) will be realized as azimuthal and radial sections of the optical module, with each XOU being an assembly of segmented Wolter-I mirrors [2]. A mechanical design of the overall mirror module based on the glass technology is being studied in collaboration with MPE and the present results confirm this is a competitive option in terms of mass and effective area [3,4].

During the last years, the realization of the XOU has been investigated with different technologies. The "Pore Optics" technology, in which a module is formed stacking special-wedged silicon wafers, is pursued in Europe by ESA [5,6]. On the other hand in USA, NASA has instead investigated the utilization of thermally shaped thin glass foils and now is working on silicon wafer slicing [7].

The replica approach represents a cost-effective solution, as several identical azimuthal sections of the mirror have to be realized. We started working on slumped technology in 2009 [8,9,10], as part of an ESA contract, which concluded in 2013. Despite the end of the contract, this development program is continued in order to verify which is the real limit of the technology. The feasibility study, led by INAF/OAB, involves also MPE and a group of industries (BCV Progetti, ADS International and MediaLario Technologies). Our approach is characterized by several innovative technical elements, concerning the technology for the hot slumping of the glass segment and their integration to form XOU.

Tens of XOUs arranged in nested rings and petals compose the final mirror assembly. Each XOU is composed of tens of tandem foils, with parabolic and hyperbolic profiles. These foils are stacked and connected together through glued glass ribs

[1] Corresponding author: marta.civitani@brera.inaf.it; phone +39-039-5971028; fax +39-039-5971000; www.brera.inaf.it

Optics for EUV, X-Ray, and Gamma-Ray Astronomy VII, edited by Stephen L. O'Dell, Giovanni Pareschi,
Proc. of SPIE Vol. 9603, 96030P · © 2015 SPIE · CCC code: 0277-786X/15/$18 · doi: 10.1117/12.2188598

that maintain the mirror foils in their mutual correct position. The position and the shape of the integrated plates are independent of the ribs, as they just depend on the position and the shape of the integration molds. The different layers are bonded with a glue layer of several microns on average: the ribs do not need to have a very accurate profile as the glue buffer compensates profile errors of the ribs up to a few tens of microns. The glass plates, shaped to a cylindrical profile with the hot slumping process, are figured to the final Wolter-I configuration through the integration process that operates as a cold slumping process by means of integration molds with parabolic and hyperbolic shapes [11]. The integration process also enables the correct relative alignment of the plates within each tandem and for the entire stack. A dedicated Integration Machine (IMA) has been designed and developed for the scope with the support of A.D.S International [12].
In this paper we present an overview of the latest activities (section 2), the results obtained in the latest integrated prototype (section 3.1) the analysis of the results (section 3.2), the proposed solution to solve the coating issue (section 4.1) and the investigation on flat integrated sample aimed to characterize the glue bonding effects (section 4.2).

2 Overview of the integrated prototypes results

Up to now, five prototypal models based on stacked slumped foils, assembled in a Wolter-I geometry have been realized using the Integration MAchine (IMA). A picture of the different assemblies is reported in figure 1, while their main characteristics are listed in Table 1.
The Proof of Concept #1 (PoC#1), realized in late 2011, was based on two plate-pair (PP) integrated in parallel configuration (figure 1A). It has been used for debugging the IMA software and the assembly procedure. The X-ray tests, performed intra-focally due to the time schedule, resulted in an inferred HEW of the plates in the range 80-120".
The XOU_BB (acronym for "X-ray Optical Unit Breadboard") has been assembled in 2012. It comprises 20 PP (3 optical + 17 dummies) in a representative mechanical configuration, including a frame in titanium representing the interface with the satellite structure (figure 1B).

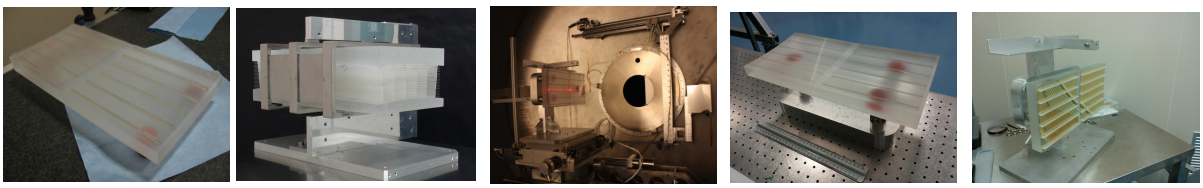

(A) (B) (C) (D) (E)

Figure 1: (A) The PoC#1 optical module. (B) The XOU_BB prototypal optical module. (C) The PoC#2 optical module during the alignment phase @Panter/MPE. (D) The PoC#3 with a single layer. (E) The PoC#4 with a coated layer.

Both the prototypes were developed following a "parallel" configuration with no common focus for the system. Moreover, the PoC#1 and XOU_BB have been assembled using low accuracy integration molds, made of Metapore and the slumped foils of D263 glass were characterized by poor optical quality. The measured HEWs at the best focus of each layer of the XOU_BB were observed to be between 48" and 60".
Nevertheless, the metrological data available on the XOU_BB layers showed clearly that the figure error of the glasses was mainly related to the integration mold. The cold slumping integration process transferred to the integrated glass foils the intrinsic error of the molds. Therefore, in order to improve the quality of the results, new integration molds have been procured: the BK7 molds were figured at Zeeko Ltd to a final HEW of around 3-4" each.
Using these new integration moulds and new AF32 glass slumped on Zerodur K20_10 mold, with better optical quality with respect to the previous segments, a new proof of concept (PoC#2) has been realized in early 2013 (figure 1C). It was based on 4 PP layers (1 dummy pair + 3 optically representative pairs). In order to check the alignment performance of the IMA, the layers were mounted in co-focal configuration. In-focus measurements were not possible for PoC#2 up to beginning of 2014 [13,14,15]: the achieved results showed a relevant step forward achieving an HEW of 22.1" in full illumination mode @0.27keV.
In order to improve further the quality of the slumped glasses, we have improved the CTE match in between glass and slumping mold by changing the glass material from AF32 to Eagle glass. Moreover a new slumping mold, with better micro-roughness with respect to the Zerodur K20_10 previously used, improved the micro-roughness of the glasses of a factor two with respect to the glasses of PoC#2 (passing from 16nm rms to around 10nm rms in WYKO range).
The prototype realized in 2014 (PoC#3), was composed of just one layer of glasses and was particularly useful to test the pencil beam characterization procedure during the X-ray test at Panter/MPE and to cross check the results with the

metrological data available for the glasses. Despite the result obtained on the whole glass (29.2" @0.93keV), a significant section of the mirrors was found well below the 10" limits confirming the potentiality of the process [2].
During the last year, the mold integration has been investigated also with the MPE glass, slumped with indirect approach and in a monolithic piece. A dedicated integration mold, made of aluminum with jointed parabolic and hyperbolic section, has been procured by MPE in LT-Ultra and used on the IMA to stack together 5 layers of glass. In order to guarantee the CTE matching between the glass (D263) and the different parts, the backplane has been realized in MPE workshop in titanium, while the ribs in BK7 procured in Helma have been used. In figure 2A is showen the stacking of the last layer of glass into the assembly. The indirect concave mold and the convex backplane support are visible. Due to the geometrical configuration of the assembly, the measure with the CUP was possible only on the backside of the latest integrated glass. In figure 2B and 2C are shown the residual with respect to the theoretical parabolic and hyperbolic shape of the two sections. As the optical surface shape can be different due to the thickness variation of the glass, this is just an indication but it fits quite well with the calibration results acquired in Panter/MPE in pencil beam. The minima in HEW are found in correspondence of the ribs, showing that for the moment the limiting factor in the assembly is the quality of the slumped glasses. Nevertheless this has been a very useful exercise to test the indirect integration mold configuration and smaller radius of curvature configuration: differently from the standard configuration used for our glasses (r=1m and F=20m), in this case the radius of curvature was 0.5m and the focal length equal to 7.4m [13].
A new integrated stack (PoC#4) based on Eagle glasses slumped on Zerodur K20 slumping mold has been as well assembled. In the next paragraphs, we will summarize the results achieved with this last PoC#4 both trough metrological characterization and trough X-ray calibration, with a critical analysis of the results.

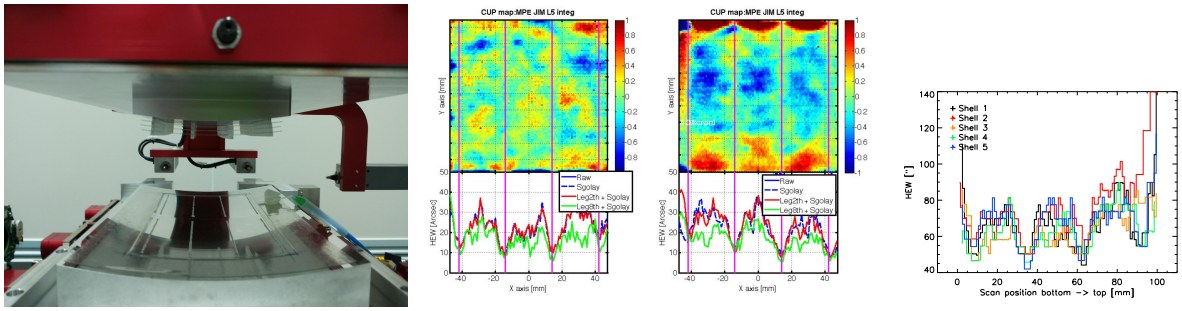

Figure 2: (A) The bonding of the last layer of the JIM. (B,C) Residual profile acquired with the CUP on the backside of the latest integrated glass and estimated HEW. (D) HEW measured in Panter/MPE on the different layers.

	PoC#1	XOU-BB	PoC#2	PoC#3	JIM	PoC#4
N° plate pairs	2	3+17	3+1	1	5	3+1
Configuration	parallel	parallel	Cofocal	Na	Parallel	Cofocal
Slumped glass material	D263	D263	AF32	Eagle	D263	Eagle
Slumping mold	Fused Silica	Fused Silica	K20_01	K20_02	…	K20_01
Integration moulds material	Metapore	Metapore	BK7	BK7	Alluminium	BK7
Integration moulds profile accuracy (equivalent HEW)	40 arcsec	40 arcsec	8 arcsec	8 arcsesc	12arcsec	8arcsec
Backplane material	BK7	BK7	BK7	Borofloat	Titanium	Borofloat
Rib material	BK7	BK7	BK7	Borofloat	BK7	Borofloat
Measured angular resolution of the prototype (HEW)	80 arcsec	60 arcsec	22 arcsec	30 arcsec	60arcsec	29arcsec
Best of the module	NA	48 arcsec	20.1	5.5arcsec	50	10

Table 1: Prototypal models realized with the Integration Machine

3 PoC#4 results and analysis

The PoC#4 is composed by 3+1 layers of Eagle slumped glasses assembled in co-focal configuration. Three layers are made of bare Eagle slumped glasses, while a dummy layer is made with the two coated glasses to experience the procedure with coated glasses.

3.1 Metrological characterization before integration

As in the other cases, the metrology of the integrated glasses has been realized with the CUP available at INAF/OAB [14]. This metrological device scans a square grid of points on the item surface. After the completion of the PoC#3, it has been decided to continue working with high resolution sampled maps scanning the glasses with 1mm sampling (instead of 5mm) in both horizontal and vertical directions. In this way it is possible to clearly highlight the defects on the glasses, distinguishing between the ones introduced during the integration and the ones already present on the glass after the slumping, improving our knowledge of the integration process. As drawback, the noise of the CHR sensor head is too high for a reliable HEW estimation and filtering process has to be operated on the data.
In figure 3A is shown a coated glass with the ribs pattern fully representative of the configuration needed for the integration into a stack. In figure 3B are reported for comparison the metrological data available for E5 and E9 before and after the coating. In the top panels are shown the low frequencies longitudinal residual of the different glasses, in the central the residual after the removal of the 2th order Legendre polynomial and on the bottom panels the residuals after the removal of the 8th Legendre polynomial to highlight the mid-frequency of the glasses, showing clearly that the mid-frequency content of the glasses are not changed by the coating. The color scale is respectively +/-4microns, +/-0.6microns and +/-0.1microns. As the low frequency errors are corrigible during the integration process, the expected HEW after the integration remains almost the same and the two glasses were considered a good test bench for the process and they were integrated as dummy layer (PP3) of the PoC#4.
The metrological characterization of all the glasses before the integration in the PoC#4 are reported in figure 4, with the same color scale of the previous figure. The measures have been acquired in vertical with the glass supported on two points on the bottom and in one point in the central part near the edge. In order to guarantee the stability of the glass during the profilometer scan, the glass is a little sustained on the back: an increase of the noise of the sensor head is recognizable in the top corner where constrains are far away. The variation of the low frequency shape is clearly visible in the passage from the E30 to the E32, in consequence of the muffle closure. All these glasses have been slumped on the K20_01 mold and are characterized by a micro-roughness of the order of 12nm in the WYKO region. More details on the slumping optimization with this kind of glass can be found in [15,16].
The expected performances of the different plate pairs were estimated trough ray-tracing simulations on the residual maps obtained after simulating the integration. The results for all the plate pairs were compatible with a global HEW around 10" @0.27keV, where the contribution of the micro roughness is estimated lower than 1arcsec.

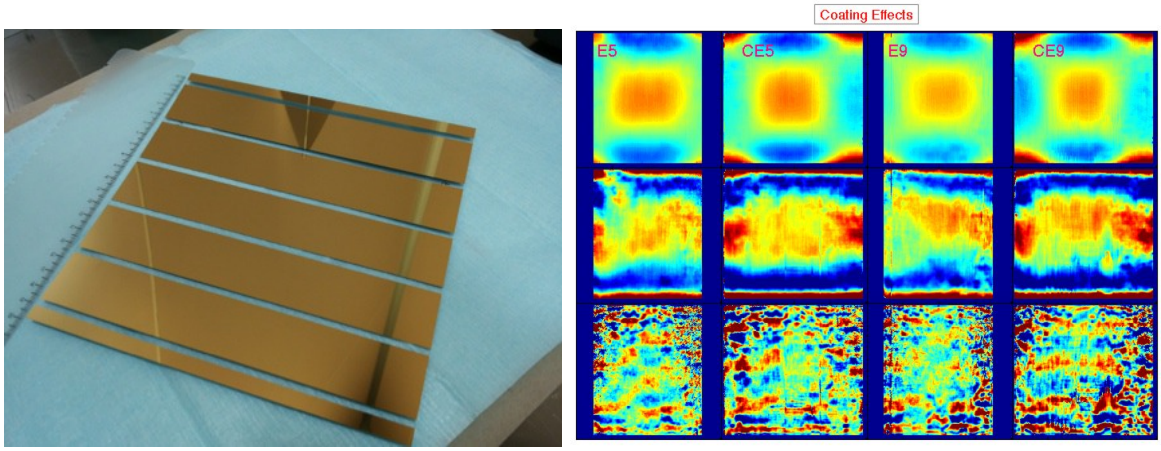

Figure 3: A glass plate (200 mm x 200 mm) slumped to cylindrical configuration (R=1m) coated with Au (150 nm, evaporated) with a pattern representative of the final configuration following the ribs. (B) The metrological data acquired before and after the coating for E5 and E9.

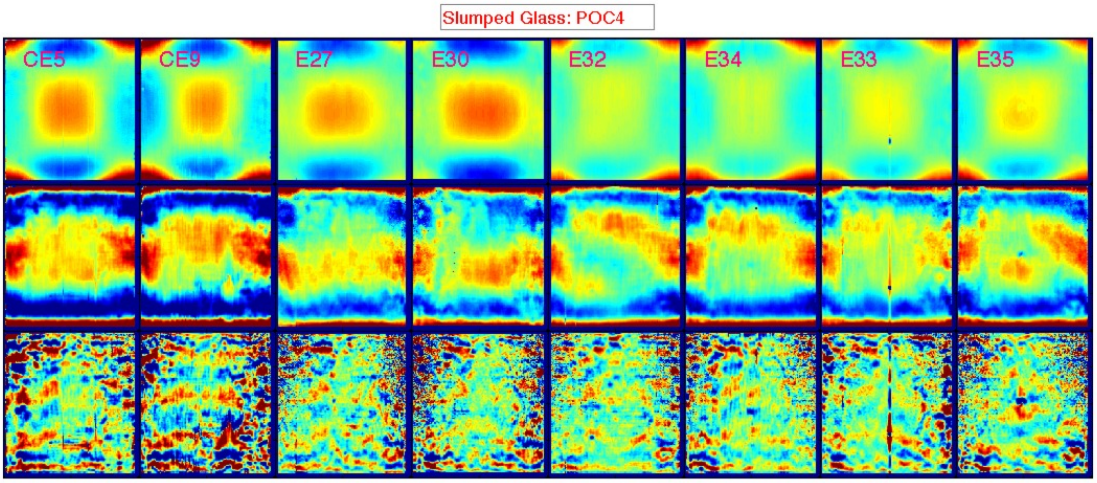

Figure 4: Slumped glass characterization before integration for the glasses composing the PoC#4. For E5 and E9, metrological data after the coating is provided. In the first line the residual errors along the longitudinal direction. The residuals after the subtraction of Legendre polynomial of the 2th order are showed in the middle, while on the bottom the residual after the removal of the 8th order.

3.2 Metrological characterization after integration

As a consequence of the stacking procedure, the external layer of a stack is the only one accessible with our metrological device. To allow the measurement, the stack has to be dismounted from the IMA. For these reasons the procedure is operated only for the last integrated layer of the stack.

In figure 5A the measurement configuration is shown, while in figure 5B and 5C the residual map (color scale is in microns) and the corresponding HEW in single reflection are reported. The resulting residual maps show clearly that one corner of the parabolic segment has been detached during the dismounting procedure. For the rest of the optical area, the resulting profile error are of around 500nm PtV with respect to the theoretical profile and the expected HEW is less than 10" for each glass: ray-tracing expected results are reported in figure 6 where they are compared with x-ray calibration results. The amplitude of the residual errors are decreased with respect to the PoC#2 and PoC#3, because of the lower initial PtV of the sag error on the slumped glass. Furthermore, in the residual maps is clearly visible the print-trough of the dust entrapped during the integration along the ribs, as well as the original defects of the slumped glass.

As for the PoC#3, the difference between the simulated and real integration in terms of HEW is in the range of 0-5" along the different scans: this integration error still takes into account the intrinsic error of the molds (estimated around 3-4" HEW each).

The major deformations on the integrated glasses are in correspondence of the dust entrapped during the integration and of the original defects of the glass. The combination of these defects prevents the glass to copy the mold figure with high accuracy disturbing the surrounding area: in the region where both the effects are absent the HEW is expected well below 10". Excluding the detached area, the achieved results on the entire glass surface are in line with the one observed in the best area of PoC#3, showing clearly that the reduction of the initial sag error of the slumped glass has a positive effect on the resulting shape of the integrated segments. In order to improve further this result, much effort should be placed in the cleaning of the slumping and of the integration process. Moreover, the figuring of the integration molds by ion beam figuring should reduce further the final residual errors on the glass.

In order to acquire information also on the innermost layers, the PoC#4 has been tested also on the UV bench available @INAF/OAB. The measurement has been repeated twice for checking the repeatability; the results are reported in figure 6 where they are compared with x-ray calibration results. In almost the cases, the values of the repeated measures are within 0.5" from the first set of values. Greater differences are evidenced on the PP3 layer, where the alignment of the mask probably hides some defects on the glass. The subtraction in quadrature of the diffraction contribution gives a resulting HEW of around 12" for all the layers apart the PP3. As the mid-frequency error of the surface is not detectable with this procedure, this remains a raw estimation of the expected HEW in x-ray. Nevertheless the results obtained are almost in line with the expected ray-tracing results on the simulated integrated maps apart for the PP3 layer.

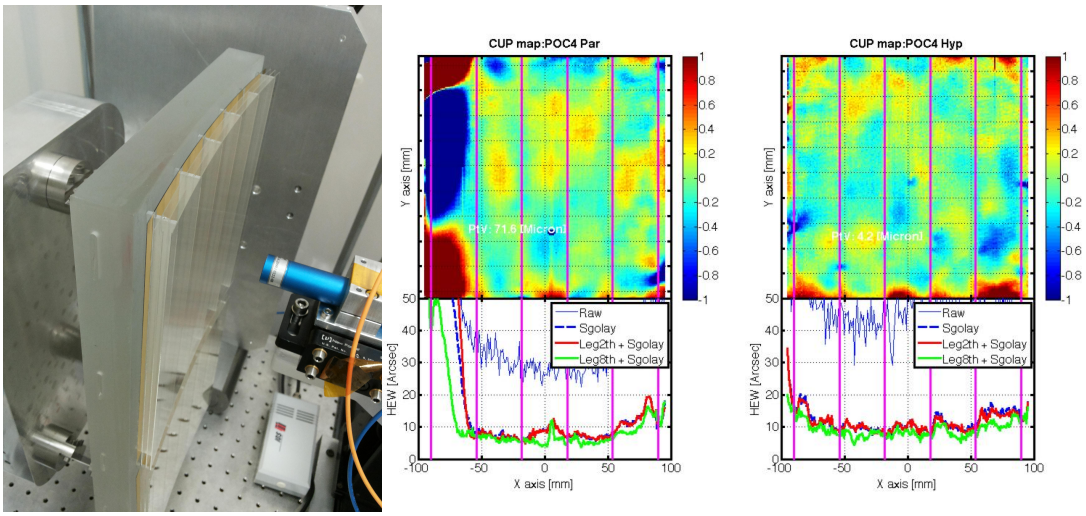

Figure 5: On the left: measured final shape and corresponding HEW of F19 and F20 (PoC#2). On the right: same measured results obtained for E16 and E18 (PoC#3).

As PP3 is the coated glass layer, some uncontrolled effect has disturbed the integration procedure. The more plausible explanation is that dust grains where entrapped between the mold and the glass at the moment of the cold shaping preparation and prevented the glass to fit the mold surface. This is a general problem for the coated glass integration and a reliable cost-effective solutions, has been found and is presented in section 4.1.

3.3 X-ray calibration: in focus measurement

The x-ray calibration of the module took place in beginning of 2015 @Panter/MPE [17]. As the 20m focal length extension was available, the measurements have been acquired with PIXI detector the module focus. Given that the optical design of the PoC#4 was identical to the PoC#2 one, the same procedure for the focus search was applied. The four layers are arranged in order overlap at the common focus of PoC#4, which corresponds to PP1 layer [18]. The best focus position for each plate pair is different along the optical axis with respect to the general one and has to be determined independently. For each single PP, isolated thought the long thin mask, several images at different focal length have been acquired with PIXI at fixed energy and the best focus position determined with the minimization of the azimuthal width of the images.
The best focus positions founded with this procedure have been used in the next to acquire the data presented in table 3. Each PP has been measured @0.27keV: for PP0, PP1 and Pp2 the resulting individual HEW are between 20.7" and 32.7" while for PP3, as expected worst with respect to the others, the results is 54". At higher energy, @1.49keV, the measured HEW are higher of around 2", slightly higher than expected from micro-roughness measurements.
In focus measurement of the whole PoC#4 results in an HEW of 32.9"; even masking the dummy layer PP3, the results do not improve so much, being above 29". This was in part unexpected with respect to the metrological data previously acquired as summarized in figure 6. The red and blue stars mark the x-ray calibration data @0.27keV and @1.49keV. The cyan bars indicate the UV data (two independent set of data for each layer, considering the whole azimuthal aperture or only the central part of the glass). In yellow are traced the corresponding inferred x-ray data, calculated removing the diffraction contribution of 16.7" in quadrature. The green circles indicate the expected HEW derived with ray-tracing on the post integration simulated maps.
The x-ray measurements confirm that the PP3 is much worst with respect to the others PPs, as expected by UV data. It is considered a useful test for the evolution of the program: it highlight that the procedure for the coated glasses need to be upgraded in order to have a reliable feedback of the imparted shaping of the glass.
The achieved results on PP0, PP1 and PP3 are higher than expected. In figure 6B, is shown the comparison between the HEW measured @Panter/MPE on the 4 layers of the POC#4 and of the PoC#2. The improvement of the micro-roughness is confirmed by the difference in HEW at different energies: for the PoC#2 glasses it was higher. For what concerns the PP0 and the PP1, the measured HEW is almost the same in the two models, while different results are observed for the PP2 and the PP3. This was not an unforeseen result as the quality of the glass before the integration is improved with respect to the ones of PoC#2. In order to understand better which kind of problem occurred during the

integration procedure, the pencil beam procedure tested on the single layer of PoC#3 has been repeated for each of the layers of PoC#4. The results are given in the next paragraph.

	HEW @0.27keV	HEW @0.93keV	HEW @1.49keV	HEW @2.98keV	Comments
PP0	20.7”		22.9”		Thin long mask
PP1	27.9”		29.5”		Thin long mask
PP2	32.7”		35.1”		Thin long mask
PP3	54.0”		57.4”	51.2”	Thin long mask
PP0+PP1+PP2+PP3	32.9”		36.5”		Full illumination
PP0+PP1+PP2	29.3”		31.8”		Full illumination

Table 2: HEW at different energies as measured in full illumination mode on the layers of PoC#4.

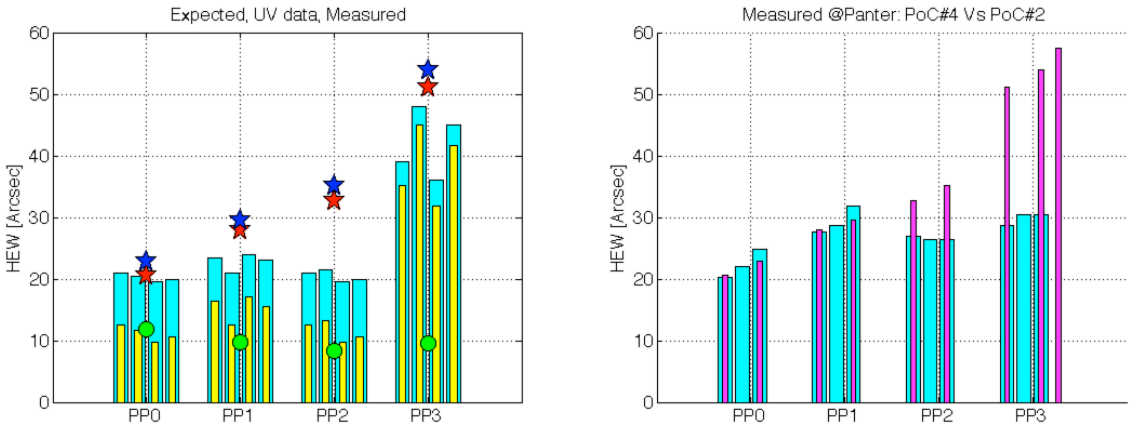

Figure 6: Left: comparison between x-ray calibration results (@0.27keV and @1.49keV, red and blue stars), the UV data (in cyan), the inferred HEW from UV data with the diffraction contribution substracted in quadrature (yellow) and from the ray-tracing on the simulated maps after the integration (green). Right: comparison between the HEW measured @0.27keV, @0.98keV and 1.49keV on the different layers of the PoC#2 (cyan) and PoC#4 (magenta).

3.4 X-ray calibration: pencil beam scans

The pencil beam procedure developed at Panter/MPE on PoC#3 [2] has to be adapted to the layers of PoC#4. Instead of having a single 20mm x2 mm slit to scan the mirror in azimuthal direction, a smaller slit of 2mm x 2.8mm has been used in such a way to isolate the different layers. The geometrical scheme followed to illuminate all the layers is reported in figure 7. The curvature along the azimuthal aperture of each layer has been followed dividing the path into 4 straight lines. The procedure for the alignment is not straightforward as the shells are quite near and only one slit has been used: as evidenced in the data acquired, part of the PP2 slit scan has been acquired in wrong position (shown in red in figure 7). In order to avoid this kind of problems in the future, a new procedure with two slits (one fixed on the plate pair and the other displaced along the azimuth) has been implemented and already tested during the JIM module calibration [13].
The measurement results available on the PoC#4 are reported in figure 8. The image of the whole scan has been created as composition of single pencil beam scans. For each pencil beam data, in the top panel it is shown the integrated intensity profile acquired (linear color scale) while on the bottom panel is indicated the corresponding HEW value. On the pencil beam scan image are overlapped (circle in magenta) the position of the baricenter along the displaced direction.
The HEW values corresponding to lower intensity level have been removed in the graph: the selection has been performed calculating for each layer the maximum intensity along the different pencil beams and then discarding the pencil beam data point with less than 60% intensity with respect to this value. The PIXI detector is not a real photon counter but ‘relative’

assessments can be performed with the same level of confidence of the HEW determination. In the top panel of figure 9 are shown the derived intensity value for each layer, while on the bottom it is reported the full set of HEW values. The correlation between the HEW and the recorded data intensity is evident and is highlighted in figure 10. The data points corresponding to higher intensity (more than 90%) correspond to an HEW of 12-22arcsec for PP0, of 16-25arcsec for PP2 and of 20-35arcsec for PP2. These 'individual beam' numbers are slightly better than the ones determined with the long slit, so that it is plausible that some effect cause wrong beam superimposition degrading the HEW of the layer when all the azimuthal aperture is considered. Moreover, from a general point of view, the better part of the glasses are in between the ribs, while the worst is the one located near the ribs. The expected effect was clearly the opposite, as in correspondence of the ribs the glasses should maintain the integration mold shape.

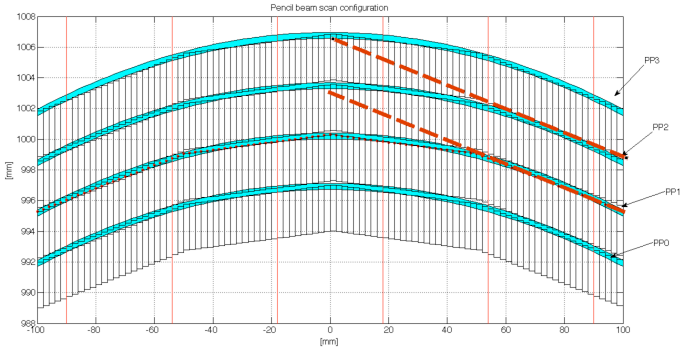

Figure 7: General set-up of the pencil beam scans. The beam width is 2mm. The strange results obtained in PP2 measurement could be explained with an error in the scanning mode as displaced in red.

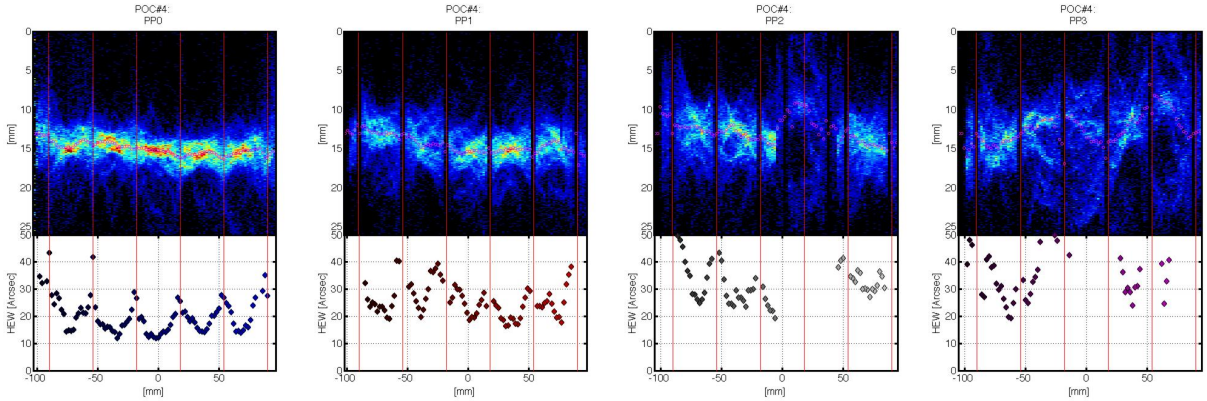

Figure 8: On the top panels, the reconstructed images at the focus of the double reflected focal spot of the PoC#4 @0.27keV. On the bottom panels, the retrieved HEW values for each beam with an intensity not lower than the 60% of the maximum found in the beam scan.

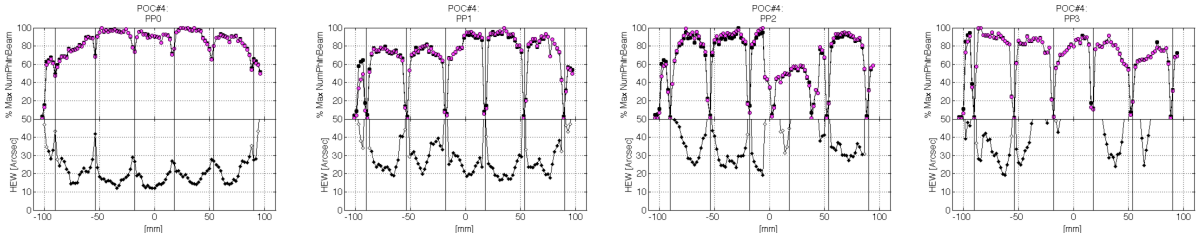

Figure 9: On the top panel, the percentage of the beam intensity with respect to the maximum one found in the same PP scan. On the bottom, the correspondent HEW values: in black the data point for which the percentage is higher than 60% while in white the discarded ones.

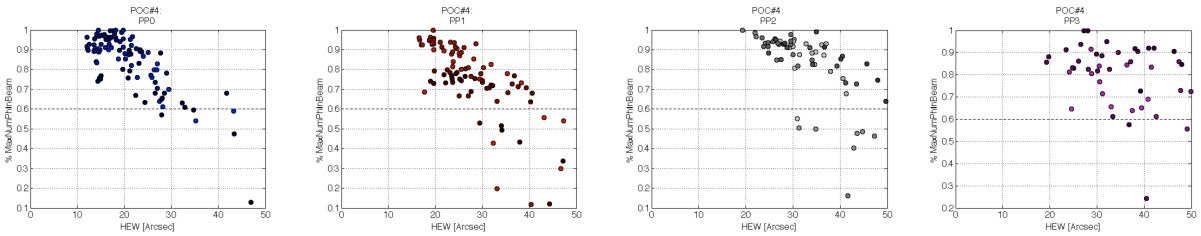

Figure 10: For each PP, the correlation between the HEW and the amplitude of the total signal in the beam.

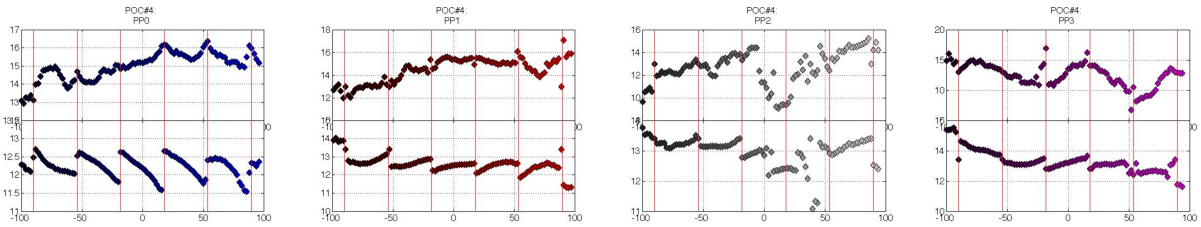

Figure 11: For each beam, on the top and on the bottom panels, the positions along the 'longitudinal' and 'transverse' direction of the beam spot barycenter as determined during the pencil beam scans.

Looking to the barycenter position of the single pencil beam scans, reported in figure 11, it is evident that a geometric effect occurred and prevented us to reach better performances. As the PP0 and the PP1 are not disturbed by error in the measurement configuration (as PP2) or by unusual optical performances (as PP3), they are used in the next to try an explanation of the results. There are jumps of around 1mm in the 'transverse' position of the baric enters, while there is a displacement of 3-4mm along the 'longitudinal' direction. The PP0 'transverse' jumps are in opposite direction with respect to the other layers one, while the trend in the 'longitudinal' direction is almost the same for the PP0 and the PP1. Ray tracing simulations have been used to understand the strange effect, assuming a perfect Wolter-I geometry and then adding an azimuthal error pattern and different misalignment of the parabolic section with respect to the hyperbolic one. The data have been divided into beams in such a way to be comparable with the pencil beam scans acquired. A sinusoidal azimuthal error pattern has been modeled with maximum (or minimum) in correspondence of the ribs positions. This pattern distributes along the 'transverse' direction the different pencil beam. The width of the composition of the foci is proportional to the amplitude of the sinusoidal amplitude: with 1micron amplitude the total width is around 0.6mm, increasing to 2.5arcsec the HEW of the global slit scan, see figure 12A. The rotation with respect to the around the Y axis of the hyperbolic section changes the focal length, maintaining the HEW contribution, see figure 12B. As well the rotation around the optical axis displace slightly the barycenter positions, see figure 12C. Instead the rotation around the axis orthogonal to the hyperbola surface spread the foci corresponding to the different beams, in 'longitudinal' direction (see figure 12D).

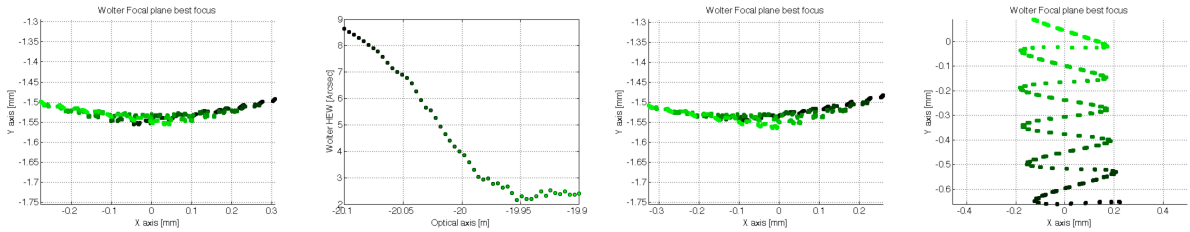

Figure 12: (A) Composition of the pencil beam spot along the azimuth, if a sinusoidal azimuthal error (with 1micron amplitude, an minimum in correspondence of the ribs) is overlapped to a perfect Wolter-I plate pair. (B) The HEW along the optical axis in correspondence of the focal plane: an additional misalignment is added to the sinusoidal pattern, so that a rotation of the hyperbolic segment that change the taper angle is introduced, and the best focus position is moved along the optical axis. (C) The composition of the pencil beam spot if a rotation along the optical axis of the hyperbolic segment is introduced.(D) The composition of the pencil beam spot if a rotation along axis normal to the hyperbolic surface is considered.

In principle, this kind of error in any case does not change the HEW of the individual beam. Additional effects are possible if, as a consequence, some parts of the glasses start to be masked or the PPs are measured off axis.

The amplitude of the total 'longitudinal' trace is proportional to the misalignment angle and sinusoids with opposite directions correspond to a reflection in the 'transverse' direction of the trace. A misalignment of 20 arcsecond spread the beam in the longitudinal direction of around 0.8mm. As the observed effect is of around 1mm in transverse direction and 3-4mm in the longitudinal one, the azimuthal pattern on the glass surface has to be of around 1micron amplitude (with opposite sign for PP0 with respect to PP1) and the misalignment of more than 80 arcsec around X.
While the azimuthal error is expected due to the glass spring back, the misalignment was not, as during the integration no particular error in the IMA algorithm was detected. Therefore after the conclusion of the x-ray calibration campaign, the alignment on the PP0 glasses has been checked. The procedure and the results are discussed in the next paragraph.

3.5 Alignment check after calibration

Due to the strange behavior of beam barycenter during the pencil beam scans, ray-tracing simulations have been tried and a similar result has been obtained in consequence of misalignments of the segments. The relative alignment between the parabolic segment and the hyperbolic segment has been checked with the UPMC machine in MLT. As the surface of the glass already integrated flex under the sensor head touch, the measuring points have been acquired only along the ribs, where the glass is more rigid. Therefore 6 scans per each segment have been acquired, all referring to the same system reference. An example of the data grid points is reported in figure 13A. Then they have been roto-traslated in order to bring the parabolic segment data in the theoretical position. At this point the roto-translation parameters to be applied in order to have also the hyperbolic segment in the Wolter-I theoretical configuration are calculated. In figure 13B is shown the hyperbolic interpolated residual in the system reference where the parabolic residua are minimized with respect to a theoretical configuration. In figure 13C is reported the interpolated results of the residual surface once the roto-translation is applied. The measurement has been repeated several times in order to check for the repeatability and the environmental effects. The results, reported in table 3, show that the results vary with the temperature but greater effect is due to the alignment of the plate pair with respect the UPMC. This last effect is probably due to the combination of the final position of the sensor head on the glass with respect to the rib and the glass bending near the ribs. As, the geometrical alignment has been carefully checked during the first measurement, while the others have been acquired in automatic procedure, this is considered the most reliable data set. In this case, the misalignment with respect to roll and pitch is of few arcsec (the imparted pitch angle for this PP0 is 17arcsec different from the PP1 reference plate pair, well in line with the measured value of 16arcsec). Instead, Yaw rotation angle is found with several tens of arcsec error. This is compatible with the effects expected from ray-tracing simulation results.

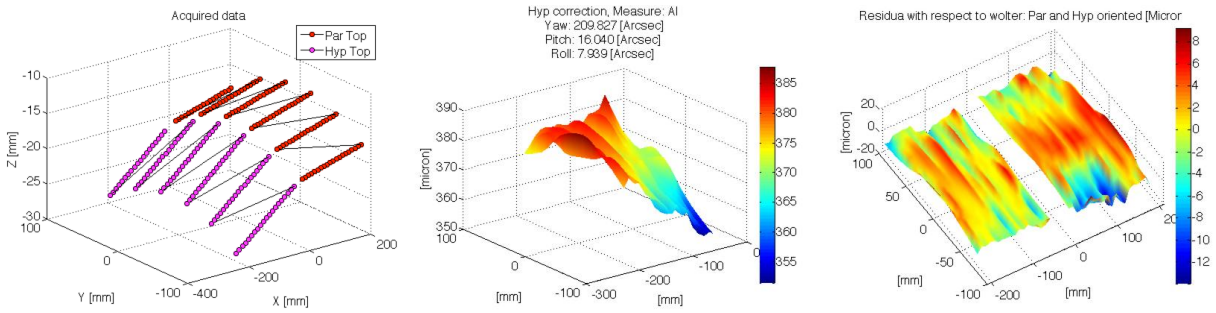

Figure 13: Left: the grid of data points acquired on parabolic and hyperbolic segments of PoC#4 PP0. Centre: the interpolated residua with respect to a theoretical Wolter-I configuration assuming perfect alignment. Right: hyperbolic residua assuming no relative rotation, the given angles give the rotations angles needed for a correct alignment.

The reason for this systematic is still unclear: a possible explanation is related to a completely wrong initial setting of the autocollimator reference value but additional test showed that the differential concept adopted for the measure make the alignment almost independent from the initial autocollimator chain alignment. Another possibility is related to a deformation of the backplane introduced during the integration for an additional weight introduced above the sensor reference frame in order to keep it more stable during the process, but also in this case FEM simulations exclude this evidence. As the UPMC measurement is limited only to the ribs area, it is also possible a misalignment of the ribs with respect to the optical axis of the mold. Due to this uncertainty, particular care has to be used in the assembly of the next prototype.

	Date	Temp.	Cleanroom environment	Yaw [Arcsec]	Pitch [Arcsec]	Roll [Arcsec]
M1	24-04-2015	23.0	Uncontrolled	209.8	16.0	7.9
M2	28-04-2015	21.0	Uncontrolled	142.6	6.3	29.1
M3	13-05-2015 9:30	19.5	Controlled	98.1	24.4	30.1
M4	13-05-2015 10:00	19.5	Controlled	96.1	21.6	25.8
M5 (realigned)	13-05-2015 10:30	19.5	Controlled	155.1	18.0	23.2

Table 3: Summary of the alignment check performed with the UPMC.

Despite the lack of improvement in terms of total HEW on the module and on the individual layers, the analysis of the results confirms that an HEW of around 10-15arcsec at low energies could be achieved starting from slumped glass of similar quality to the ones of PoC#4. This statement should be confirmed, before the prosecution of the activities with different glasses, through the re-assembly a new PoC with the same glasses but preventing misalignment errors. At the moment the PoC#4 has been already dismounted, the backplane remounted on the IMA and is ready to be re-assembled, but as glue residua are still present on the glasses the activity will be carried out as soon as a more effective procedure to clean the glasses will be operated.

4 Further developments

Different activities have been done and are currently on going to up-grade the technology and to acquire a better comprehension of the process. They are reported in the next paragraphs.

4.1 Dust particle detection process for coated glass segments

Up to the integration of PoC#3, the slumped glasses have been measured in X-rays thanks to the good reflectivity of the bare glass at low energies, as they were not coated. Nevertheless, in the XOU development process, the glass plates should be coated after the slumping and the cutting procedure. Depending on the material used for the coating, the thickness and the adopted process, the stresses on the glass could be different resulting in different deformation of the glasses. Moreover to allow the bonding of the stacked layers a gap in correspondence of the ribs should be left coating-free. While a systematic work to evaluate the effects of the coating has been initiated on our slumped glasses [2], the operational problem that could arise during the integration of this kind of segments has been verified during the assembly of PP3 of PoC#4.

Different variables concur to the quality of the cold slumping replica, like the rigidity of the structure, the fixture pattern and the bonding shrinkage. On the top of those, it is fundamental that the surface of the thin sheet replicates as much as possible the surface of the reference. A major operational problem is the entrapping of dust grains between the two surfaces: in this case the thin sheet is prevented to get the reference shape and replica cannot be perfect.

Our process is performed in a clean room environment; nevertheless we already noticed the presence of residual contamination on bare glass. Its cleanliness level can be improved, but achieving the desired level of cleanliness trusting only on the ambient control can be extremely expensive.

The workout solution, that we have experienced, is to repeat the process under an air flow as many times as needed (in general few times) with a feedback to evaluate the amount of dust present in order to identify the part of the sheet or of the mould to be re-cleaned to guarantee a better contact between the parts.

When the thin sheet is made of transparent material, as glass for example, the dust presence can be checked looking to the interference fringes of the two surfaces layers where they appears as concentric circles around the points where dust is present (figure 14). In this case the positioning of the item on the reference can be repeated until the desired cleanliness level is reached.

Instead, when the thin sheet is not transparent, as in the case of coated glass, there is no way to highlight the dust presence and therefore there is no way to verify the achievement of the desired cleanliness level. As the results obtained on the coated layer of the PoC#4 were not encouraging, we had to find a solution for this issue that could be a bottleneck for the whole process.

We find a solution by means of deflectometry technique used in differential mode. Comparing the image of the reflected pattern from the reference mandrel surface with the reflected pattern recorded after the thin sheet positioning, the bump of

the dust grain will be easily highlighted: the dust presence appears in the measurement as a higher frequency slope error variation in correspondence to the dust grain.
This type of measurement is extremely versatile as can be adapted to whatever reference mandrel shape: a null-measurement of the mandrel is taken before the start of the actual measurement series. Thanks to this differential concept it is intrinsically free form and using multiple camera it is possible to map whatever mirror shape. Furthermore, as anticipated, it overcomes all problems due to the systematic errors due to the alignment of the parts.
This is a very cost effective solution as the same flexibility would be extremely costly to achieve with any other metrological solution (e.g. Interferometry or coordinate measurements machine CMM). An inteferometric setup, which can achieve the same nearly instantaneous acquisition and high resolution, would be more than a factor 100 costly. Apart from the interferometer itself, a null lens would be needed for every major change in surface shape. On the other side, a CCM would need several hours for scanning a surface at comparable resolution.

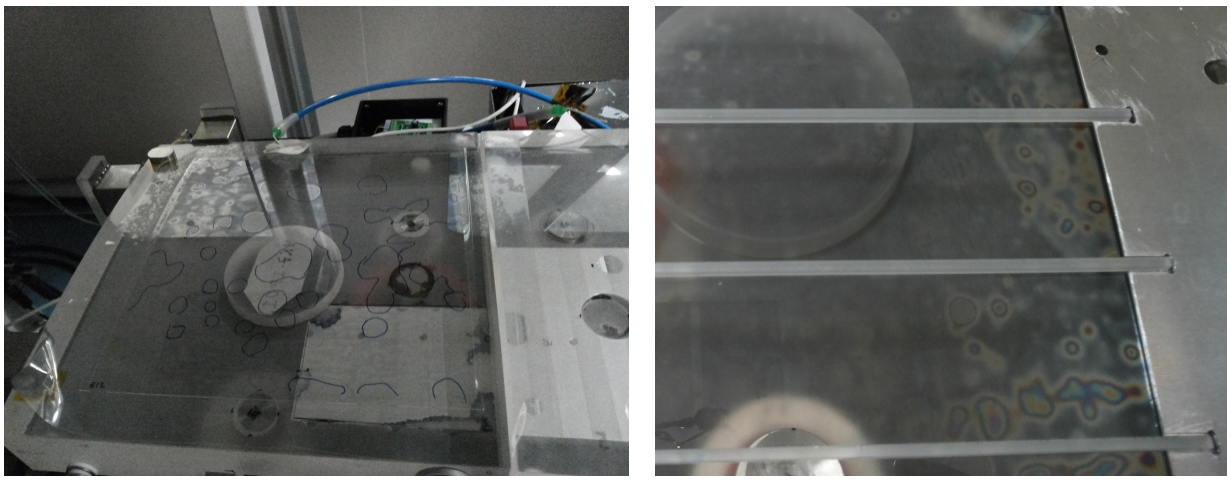

Figure 14: Left: the reference mandrel made in BK7 with an uncoated thin glass sheet (0.4mm thickness) kept in contact with the surface trough vacuum suction. The zones where the dust grain presence prevents the complete contact are highlighted with a pen on the glass surface. Right: a detail of the visible fringes.

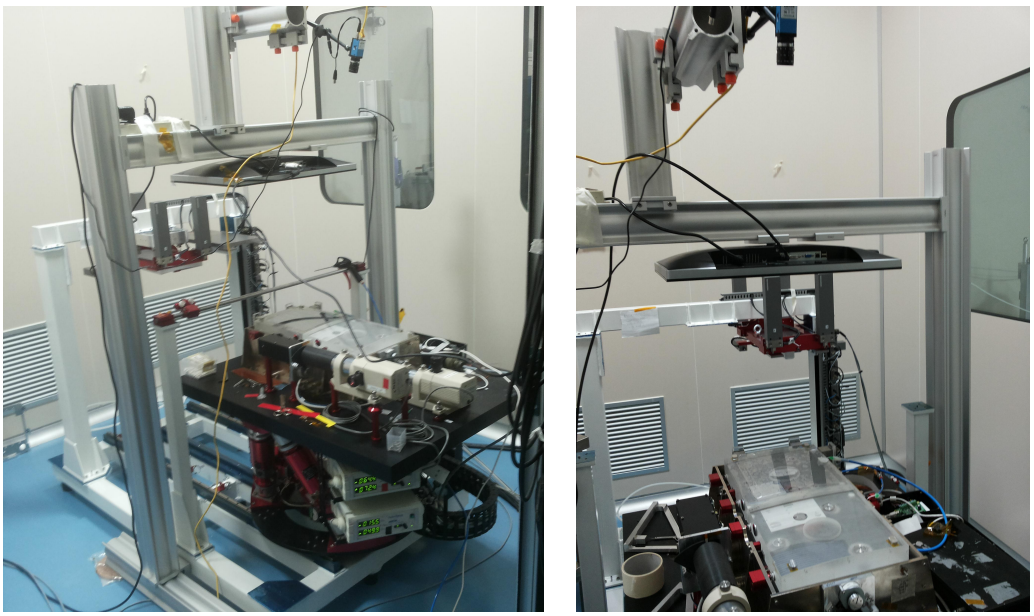

Figure 15: The deflectometry set-up used for the test. A screen and a camera looking to the surface are placed above the surface to be checked. An initial measure is acquired on the reference surface: once the thin glass is placed above it, the difference with respect to this measure will be considered.

The applicability is not limited to cold slumping processes: it is conceivable to use this technique anytime it is necessary to check the correspondence between a master surface and a child surface copying the master. A first example could be a quick verification of the accuracy of the replica for a glass after a hot slumping process: the measure of the surface before removing the glass from the mold is compared with the one of the forming mold. A different application could be during the machining of glass/wafer to reach constant thickness. In the case of the glass for example, the part to be machined is placed in full contact with a flat reference and then is machined on the other side. With a deflectometric device, working in differential way with respect to the reference, it is possible to easily monitor the evolution of the thickness variation in real time without moving the item from the reference.
The concept has been already validated on the Integration Machine set-up @INAF/OAB. The deflectometry system set-up has been realized using the equipment and the control SW developed in MPE for the metrology post integration of thin slumped glasses [19]. A picture of the new IMA set-up is shown in figure 15.
As an example, in figure 16 the results achieved for a bare glass are shown, where we had the opportunity to compare our previous dust detection method, with the results given by the deflectometric system. As this was a trial for the system, we did not took particularly care about the amount of dust entrapped; we just took care of tracing with a marker on the surface the contaminated areas. The correspondence between the two is complete, apart for a residual systematic waviness error that does not prevent the recognition of the dust positions.
In figure 17 similar results are showed obtained on a fully coated glass and on the E5 glass after the PoC#4 dismounting. In this case the glue residua on the ribs pattern are clearly individuated from the system and prevented the planned re-bonding of the glass as test verification procedure. Moreover the different 'random' dust positions are clearly recognizable. In view of an automatic integration procedure, this procedure can be particularly useful to optimize the set-up of the glass before the bonding.

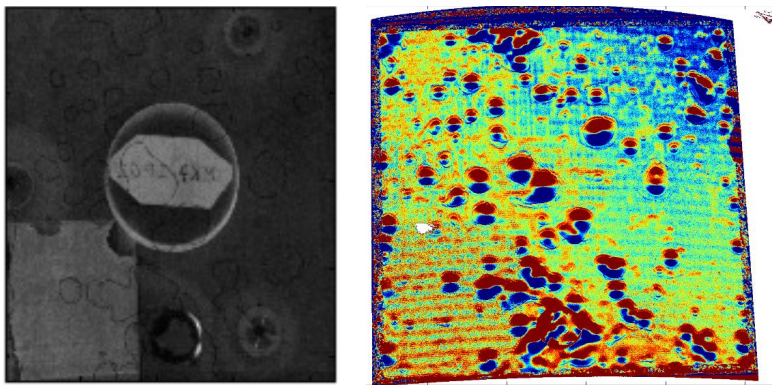

Figure 16: Left: enlarged images of the dirty areas. Right: in the output of the differential measurement, the high frequency variation along the vertical direction corresponds to the highlighted areas.

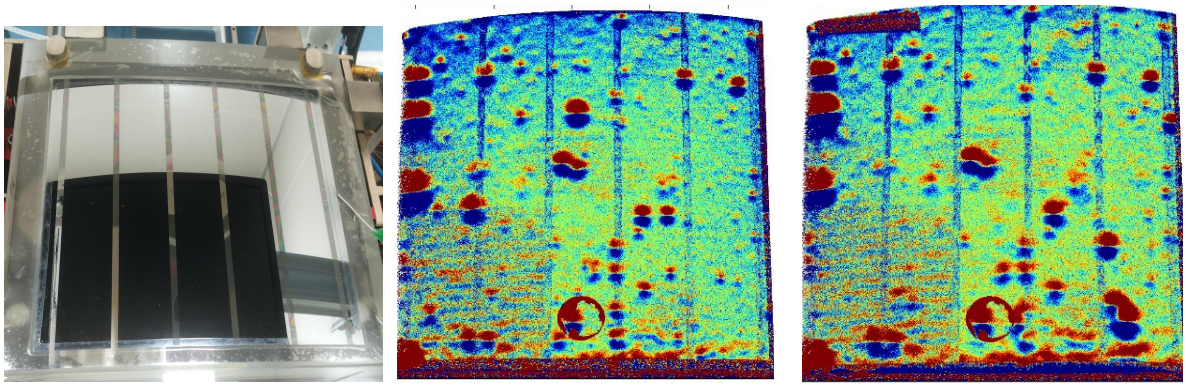

Figure 17: Left: when a coated glass is placed above the reference, the coating prevents the cleanliness check. Right: Indications of the dust presence and position can be retrieved with the deflectometry set-up: different set-up of the glass results in different pattern.

4.2 Bonded ribs effect evaluation

The analysis of the pencil beam scans shows an increase of the HEW in the region near the ribs. In order to have an alternative evidence that the observed effect was not linked to the bonding procedure, it has been carried out a detailed analysis on integrated samples assembled with different amount of glue and glue distribution prescriptions. The samples have been made with flat glasses 100mm x100mm, using a flat reference as integration mold and three ribs at a distance of 30 mm. An image of the sample is reported in figure 21A. After the integration, the shape of the glass has been measured with the interferometer (thanks to a coating layer deposited on the glass).

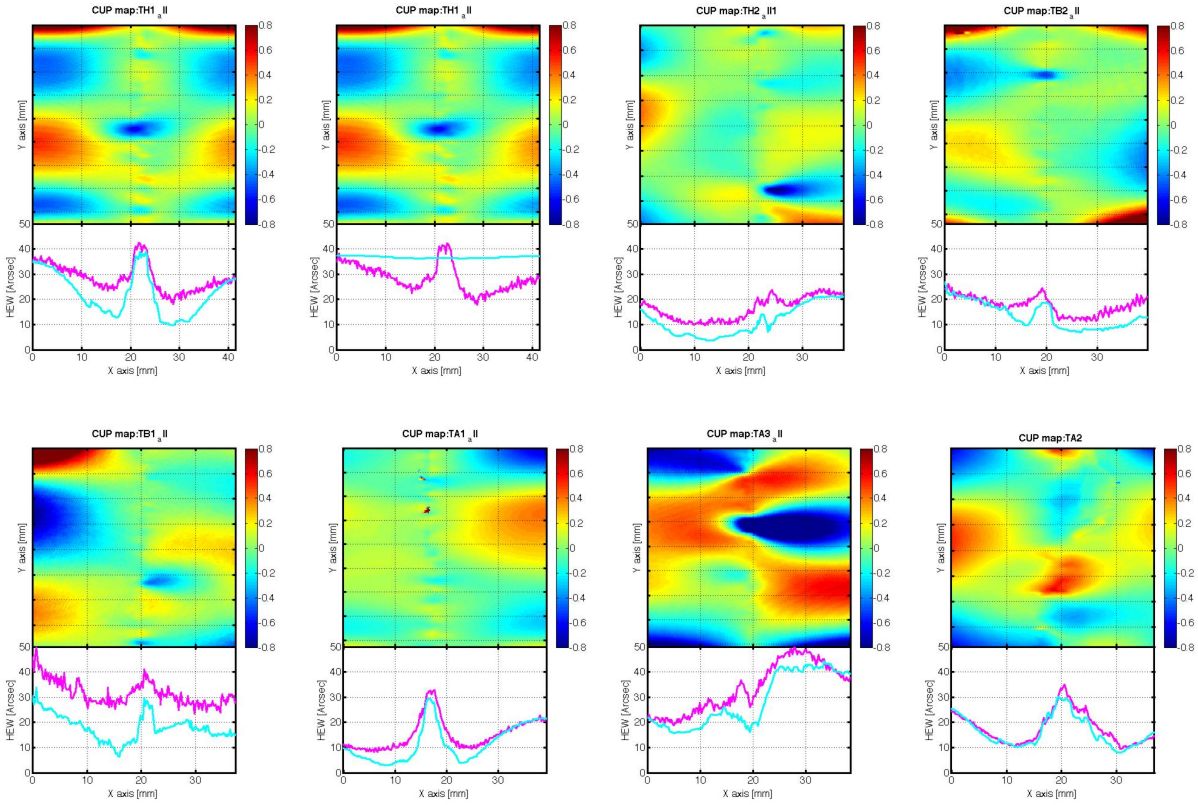

Figure 18: Interfereometric measurement of the integrated samples: TH1 and TH2 (50 microns of glue overflowing from the rib), TA1, TA2 and TA3 (100micron of glue well distributed) and TB1 and TB2 (50micron of glue well distributed).

The data acquired over a circle of 100mm diameter, have been cut in a square in order to isolate the deformations under the central rib and the residua analyzed with ray tracing and Fresnel algorithm. Due to the huge initial figure error (low frequency) of the glass, the overall mirror shape error is not representative for the integration concept. Instead the local deformations in correspondence of the ribs give an idea of the rib bonding effects. The results are shown in figure 18. The samples TH1 and TH2 have been bonded with improper glue distribution accuracy (50micron thick and exceeding the ribs width), while for the other the glue distribution has been carefully controlled but with different thickness (TA2 and TA3 with 100 micron while TB1 and TB2 with 50micron). On the top panel is shown the measured error shape in the central region of the plate, where the central rib is present. The colorscale is in micron. On the bottom panel there is the HEW estimation along the vertical scan line, both trough ray-tracing (magenta) and Fresnel algorithm (cyan) [20]. The calculation has been performed in all the cases at 0.27keV, while for the sample TH1 the comparison of the expected HEW results under UV light is presented. In UV light, due to the diffraction, the ribs position is not recognizable, while in x-ray measurement the rib feature is clearly visible. In this case, due to the size of the mirror, the amplitude of the diffraction effect is greater than for PoC plates, but it is the same kind of effect. In the region above the ribs, ripples are generated on few millimeters scale. The amplitude of the effect depends on the amount of glue used for the bonding. In order to allow a comparison, the height and the width of the HEW peak in correspondence of the rib have been summarized in figure 19.

The maximum value of the HEW on the peak (note that in any case this is not optical area for the mirror) is around 30arcseconds in all the cases, with higher variability observed when the glue distribution is not carefully done. Instead, the width of the peak is depending more strictly on the thickness of the layer: the smaller the amount of glue, the smaller is the area interested. In this case the area affected by the local deformation of the glue is around 5mm, while the maximum size of the affected area is between 10mm and 20mm.

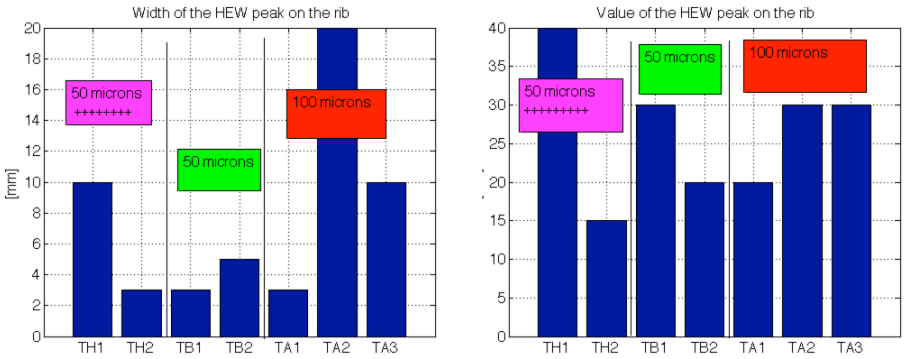

Figure 19: The width of the HEW peak and the HEW maximum value in the different bonded samples.

These results are almost in line with the ones achieved during x-ray measurement of PoC#2, where a mask with dedicated pattern has been used to isolate the regions of the glasses near the ribs. The size of the unmasked region near the ribs is 10mm. The resulting HEW values derived are summarized in figure 20. For the innermost layer, the measured HEW is higher near the ribs with respect to the whole glass with values around 30-35 arcsec. In all the cases, apart for PP3, this is the better region of the glass, so that the ribs bonding was not the driving factor in the PoC#2 global performances. In any case, it is expected that a better control during the glue distribution would concur to improve the quality of the future prototypes and for this reason should be pursued.

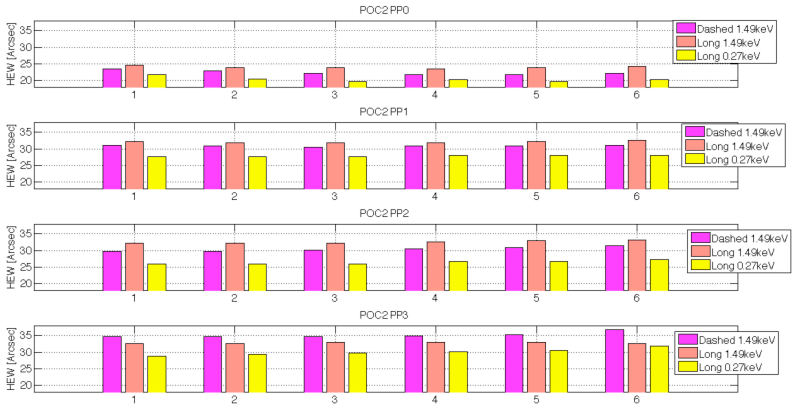

Figure 20: HEW measured @Panter/MPE during PoC#2 calibration. The data compared have been acquired with long slit @0.27keV, @1.49keV and with dashed mask to isolate the ribs region @1.49keV.

During the stack assembly, the ribs are bonded to two glasses: in one case during the glue curing time the glass is maintained forced in contact with the mold by the vacuum suction (as in the test cases presented before), while in the other the glass is integrated in the stack and in principle its shape can be deformed with the glue shrinkage, as it is constrained only in correspondence of the previously bonded ribs. In order to analyze the possible effects in this different bonding configuration, a dedicated test configuration has been foreseen with the usage of the deflectometric set-up presented in the previous paragraph. Preliminary tests are being carried out on flat samples in order to evaluate the sensitivity and the accuracy of the system. In figure 21, are shown the measurement configuration and the final deformation observed on a sample in terms of slope variations. The sample is one the already bonded samples used for previous tests. While the shape of the optical surface is measured at fixed temporal interval with the deflectometric set-up, a new rib is bonded over the optical surface in correspondence of the central rib used for assembling the glass with the backplane. In this case, higher

deformations are visible in correspondence of the calibrated wire (100microns) used to fix the distance between the rib and the glass. Furthermore, the effect is not symmetric with respect to the position of the central rib probably due to the manual procedure used for align the new rib over the one already present under the glass. In this case the area interested by the deformation is maximum 10mm width: this result is in line with all the other indication retrieved, but it needs to be sustained by a dedicated test campaign that will be carried out in the next months.

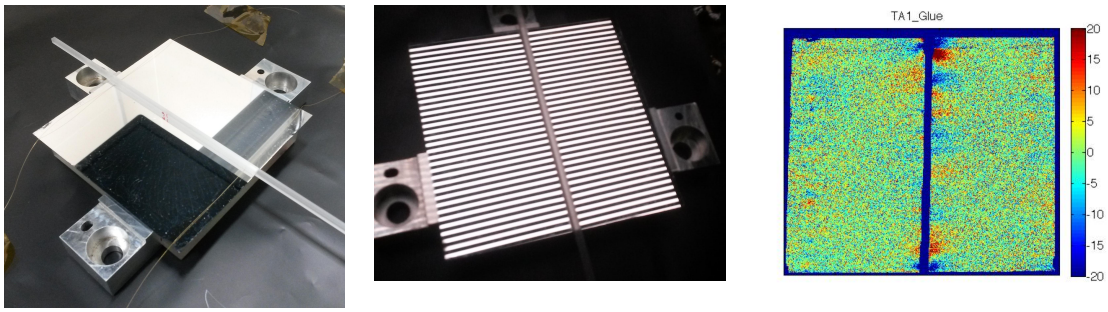

Figure 21: (A) An additional rib is bonded in the central part of the previously integrated glass. (B) The fringes projected by the deflectometric system to control the deformations on the glass surface due to the glue shrinkage. (C) The difference in the angular slope error between the initial and the final data acquired after 8.5 hours.

4.3 Conclusions

In order to proof that the SGO technology has the potential to make the mirror units needed for ATHENA, the effort in realizing and testing prototypal optics unit is continuing. During the last year two mirror stacks have been assembled by means of the IMA following the integration scheme based on the cold slumping approach. In one case, the 'inverse' integration concept has been tested for the first time, using indirect slumped glasses produced by MPE and concave monolithic integration mould.

In the other case, four layers of glasses slumped in cylindrical configuration with the INAF/OAB approach has been assembled in a PoC#4. In this case, the novel factors were a better quality of the slumped glasses (EagleXG glasses slumped on Zerodur K20 mould) and the introduction of a coated layer to test the integration procedure for the future development of the program. The x-ray measurement campaign showed that with the present direct slumping configuration the mirror micro-roughness remains an issue if the quality of the slumping mold is not optimal: in this case an additional 2" error in HEW going from 0.27 to 1.49 keV has been introduced being the glass figured with an old slumping mold with σ =20nm rms on millimiter scale. The global HEW of the integrated PPs was unexpectedly not better than the PoC#2. Nevertheless the pencil beam data acquired on PP0 showed that between the ribs the glass easily reach 10-15" HEW. This is pretty in line with PoC#3 results: in that case, on one side of the PP, between the two external ribs, the HEW was well below 10" both at 0.27 and at 1.49 keV, indicating clearly the potentiality of the system. In that case the initial sag error of the glass was around 8 micron PtV in the central part, so that the its correction was possible only on the sides, where the integration correction is more effective. Now that the longitudinal sag error has been decreased to 2-4microns, the results are correspondently improved on the whole width of the plate.

Unfortunately, the unusual geometric composition of the focal spot has been correlated, after the calibration completion, with a misalignment of the parabolic and hyperbolic segment that prevented the achievement of global reliable results. The prototype has now been dismounted and its reassembly will be operated.

The results achieved on the integrated coated layer evidenced the need for an upgrade in the process in order to avoid the dust grains, entrapped between the glass and the integration mold and not visible under the coating, destroy the quality of cold shaping of the glass. A cost-effective solution has been found and already implemented on the IMA. It is based on the deflectometry approach and guarantees good dust grain traceability. The present configuration will remain part of the IMA. Moreover a new deflectometric set-up will be realized in the next months to allow a preliminary measurement of the integrated glass without dismounting the stack. This new device is expected to be very useful as no metrological data is at moment available for the innermost layer integrated and can be used for a systematic comparison of the shape of cylindrical glass before and after the bonding of a new set of ribs over it.

Additional activities are foreseen in collaboration NFC/NASA. Given that the radius of curvature and the focal length is different from our (R= 243mm and F=7.4m), a new set of integration molds is needed to try the cold slumping integration concept on their slumped glasses. In an initial phase, these molds will be provided by MPE and realized in alluminium. While the first integrated module will be used for checking the procedure and the metrological set-up, new BK7 integration

molds will be realized in INAF/OAB laboratories by means of the new Zeeko machine recently acquired (RefVecchi2015). As the intrinsic quality of the glasses is given around 6" in double reflection, these substrates are ideal to demonstrate the entire potential of the process.

Acknowledgments

Many thanks go to M. Tintori, P. Fumi, and G. Gallieni, (ADS International) and to all OAB staff (in particular to S. Cantù and E. Mattaini of the OAB mechanical workshop) for their valuable support.

References

(1) K. Nandra, X. Barcons, D. Barret, A. Fabian, J.W. den Herder, L. Piro, M. Watson "Athena: The Advanced Telescope for High Energy Astrophysics," Mission proposal, http://www.the-athena-x-ray-observatory.eu/
(2) M. M. Civitani, M. Ghigo, G. Pareschi, B. Salmaso, D. Spiga, G. Tagliaferri, G. Vecchi, V. Burwitz, G. D. Hartner, B. Menz, " X-ray optical units made of glass: achievements and perspectives," Proc. SPIE 9144, 914416 (2014)
(3) S.Basso, E.Buratti, M.M.Civitani, G.Pareschi, B.Salmaso, D.Spiga, G.Tagliaferri, J.Eder, "A high resolution large x-ray mission based on thin glass: optomechanical design", Proc SPIE 9144, (2014)
(4) S. Basso, M. M. Civitani, G. Pareschi, E. Buratti, J. Eder, P. Friedrich, M. Fürmetz, "A design study of mirror modules and an assembly based on the slumped glass for an Athena-like optics", Proc SPIE 9603, (2015)
(5) M. J. Collon; S. Kraft; R. Günther; E. Maddox; M. Beijersbergen; M. Bavdaz; D. Lumb; K. Wallace; M. Krumrey; L. Cibik; M. Freyberg, "Performance characterization of silicon pore optics", Proc. SPIE 6266, (2006)
(6) M. Bavdaz, N. Rando, E. Wille, K. Wallace, B. Shortt, M. Collon, C. van Baren, G. Pareschi, F. Christensen, M. Krumrey, M. Freyberg, "ESA-led ATHENA/IXO Optics Development Status", SPIE 8147, 81470C (2011).
(7) W. W. Zhang, M. P. Biskach, V. T. Bly, et al., "Affordable and lightweight high-resolution x-ray optics for astronomical missions," Proceedings of SPIE Vol. 9144, 914415 (2014)
(8) M. Ghigo, S. Basso, R. Canestrari, P. Conconi, O. Citterio, M. M. Civitani, E. Dell'Orto, D. Gallieni, G. Pareschi, G. Parodi, L. Proserpio, D. Spiga, "Hot slumping glass technology and integration process to manufacture a grazing incidence scaled prototype for the IXO telescope modules", Proc. SPIE 7437, (2009)
(9) M. M. Civitani, S. Basso, M. Bavdaz, O. Citterio, P. Conconi, D. Gallieni, M. Ghigo, B. Guldimann, F. Martelli, G. Pagano, G. Pareschi, G. Parodi, L. Proserpio, B. Salmaso, D. Spiga, G. Tagliaferri, M. Tintori, E. Wille, A. Zambra, "IXO x-ray mirrors based on slumped glass segments with reinforcing ribs: optical and mechanical design, image error budget, and optics unit integration process", Proc. SPIE 7732, (2010)
(10) G. Parodi, F. Martelli, S. Basso, M. Bavdaz, O. Citterio, M. M. Civitani, P. Conconi, M. Ghigo, G. Pareschi, L. Proserpio, D. Spiga, E. Wille, A. Zambra, "Design of the IXO optics based on thin glass plates connected by reinforcing ribs", Proc. SPIE 8147, (2011)
(11) M. M. Civitani, S. Basso, O. Citterio, P. Conconi, D. Gallieni, M. Ghigo, G. Pareschi, L. Proserpio, B. Salmaso, G. Sironi, D. Spiga, G. Tagliaferri, A. Zambra, F. Martelli, G. Parodi, P. Fumi, M. Tintori, D. Gallieni, M. Bavdaz, E. Wille, "Accurate integration of segmented x-ray optics using interfacing ribs", Opt. Eng. 52(9), 091809-091809, (2013)
(12) M. M. Civitani, S. Basso, M. Bavdaz, O. Citterio, P. Conconi, D. Gallieni, Ghigo, M., B. Guldimann, F. Martelli, G. Pagano, G. Pareschi, G. Parodi, L. Proserpio, B. Salmaso, D. Spiga, G. Tagliaferri, M. Tintori, E. Wille, A. Zambra, "An integration machine for the assembly of the x-ray optic units based on thin slumped glass foils for the IXO mission," Proc. SPIE 8147, 81470R (2011)
(13) L. Proserpio, E. Breunig, P. Friedrich, A.Winter, C. Rohé, J. Eder, V. Burwitz, G. D. Hartner, B. Menz, M. M. Civitani, S. Basso, E. Buratti, "JIM: a joint integrated module of glass x-ray optics for astronomical telescope," Proc. SPIE 9603, (2015)
(14) M. M. Civitani, M. Ghigo, O. Citterio, P. Conconi, D. Spiga, G. Pareschi, L. Proserpio, "3D characterization of thin glass x-ray mirrors via optical profilometry," Proc. SPIE 7803, 78030L (2010)
(15) M. Civitani, M. Ghigo, S. Basso, L. Proserpio, D. Spiga, B. Salmaso, G. Pareschi, G. Tagliaferri, V. Burwitz, G. D. Hartner, B. Menz, M. Bavdaz, E. Wille, "Direct hot slumping and accurate integration process to manufacture prototypal X-ray Optical Units made of glass," Proc. of SPIE Vol. 8861 886110-1 (2013)
(16) B. Salmaso, C. Brizzolari, S. Basso, M. Civitani, M. Ghigo, G. Pareschi, D. Spiga, G. Tagliaferri, "Slumped glass

optics for x-ray telescopes: advances in the hot slumping assisted by pressure," Proc. SPIE 9603, (2015)
(17) V. Burwitz, M. Bavdaz, G. Pareschi, M. Collon, W. Burkert, M. D. Ackermann, G. Hartner, D. Spiga, M. M. Civitani, B. Menz, "In focus measurements of IXO type optics using the new PANTER x-ray test facility extension," Proc SPIE 8861-51, (2013)
(18) M. M. Civitani; P. Conconi; G. Pareschi, "Cost-effective design and simulations for a prototypal x-ray optical unit for the IXO telescope," Proc SPIE 8141, 81410M (2011)
(19) E. Breunig et al.," Characterising x-ray mirror deformations with a phase measuring deflectometry system," Proc. SPIE 9144 (2014)
(20) D. Spiga, S. Basso, M. Bavdaz, V. Burwitz, M. Civitani, O. Citterio, M. Ghigo, G. Hartner, B. Menz, G. Pareschi, L. Proserpio, B. Salmaso, G. Tagliaferri, E. Wille, "Profile reconstruction of grazing-incidence x-ray mirrors from intra-focal x-ray full imaging," Proc. SPIE 8861, 88611F (2013)